Pramana – J. Phys. (2016) 87: 57
DOI 10.1007/s12043-016-1248-0

Structural, morphological, optical and antibacterial activity of rod-shaped zinc oxide and manganese-doped zinc oxide nanoparticles

A DHANALAKSHMI[1], B NATARAJAN[2,*], V RAMADAS[3], A PALANIMURUGAN[4] and S THANIKAIKARASAN[5]

[1]Research & Development Centre, Bharathiar University, Coimbatore 641 046, India
[2]PG & Research Department of Physics, Raja Doraisingam Government Arts College, Sivagangai 630 561, India
[3]PG & Research Department of Zoology, Raja Doraisingam Government Arts College, Sivagangai 630 561, India
[4]PG & Research Department of Chemistry, Raja Doraisingam Government Arts College, Sivagangai 630 561, India
[5]Centre for Scientific and Applied Research, School of Basic Engineering and Sciences, P.S.N. College of Engineering and Technology, Thirunelveli 627 152, India
*Corresponding author. E-mail: b_natraj_b@rediffmail.com

MS received 11 May 2015; revised 4 December 2015; accepted 16 December 2015; published online 21 September 2016

Abstract. Pure ZnO and Mn-doped ZnO nanoparticles were synthesized by Co-precipitate method. The structural characterizations of the nanoparticles were investigated by X-ray diffraction (XRD) and scanning electron microscopy (SEM) techniques. UV–Vis, FTIR and photoluminescence (PL) spectroscopy were used for analysing the optical properties of the nanoparticles. XRD results revealed the formation of ZnO and Mn-doped ZnO nanoparticles with wurtzite crystal structure having average crystalline size of 39 and 20 nm. From UV–Vis studies, the optical band-gap energy of 3.20 and 3.25 eV was obtained for ZnO and Mn-doped ZnO nanoparticles, respectively. FTIR spectra confirm the presence of ZnO and Mn-doped ZnO nanoparticles. Photoluminescence analysis of all samples showed four main emission bands: a strong UV emission band, a weak blue band, a weak blue–green band and a weak green band indicating their high structural and optical qualities. The antibacterial efficiency of ZnO and Mn-doped ZnO nanoparticles were studied using disc diffusion method. The Mn-doped ZnO nanoparticles show better antibacterial activity when higher doping level is 10 at% and has longer duration of time.

Keywords. ZnO; nanoparticles; X-ray spectra; optical properties; biomaterials.

PACS Nos 78.20.Ci; 78.67.Bf; 32.30.Rj; 78; 87.85.J–

1. Introduction

In the recent decade, one of the most significant challenges faced by the world is the recurrence of infectious diseases and the bacterial contamination in all kinds of materials [1]. Several antibacterial agents are widely used in day-to-day life for the prevention of infectious diseases and bacterial contamination [2]. When antibacterial agents are used in the new packaging materials for health care and food applications, the most crucial parameters to be taken care of are low toxicity to human beings and high efficiency in controlling bacteria. Inorganic antibacterial agents are increasingly used because of their creditability and stability when compared with organic antibacterial agents. New nanostructured materials with antibacterial properties are the need of the day for preventing microbial growth because the size, structure and surface properties of nanomaterials can improve the antimicrobial efficacy [3]. Several inorganic metal oxides such as TiO_2, MgO, ZnO and CuO have gained increasing attention in recent years. Of these oxides,

ZnO is a versatile and important semiconducting material with a band gap of 3.37 eV that can exhibit some special features like excellent chemical and thermal stability, high transparency and biocompatibility. ZnO has attracted much attention from the industry, as it is suitable for many potential applications in optoelectronic devices [4], sensors [5], dye-sensitized solar cells [6], biodevices [7] and photocatalysts [8]. Moreover, various morphologies of ZnO such as nanowires [9], nanorods [10], nanotubes [11], nanowhiskers [12] and nanoflowers [13] have been found to be useful in biomedical applications. The characteristics of ZnO, ZnO nanoparticles and Mn-doped ZnO nanoparticles suitable for biomedical applications demand precise control of particle size, shape and preparation conditions that influence these properties. Different physical or chemical synthetic methods have been used to prepare doped ZnO nanoparticles [14–20]. Coprecipitation is one of the most important methods to prepare nanoparticles in large scale with low cost. In order to enhance the optical properties and obtain a small particle size, a search for alternative synthesis methods for efficient Mn doping with ZnO nanoparticles has become the major interest of studies with high surface area for better antibacterial performance using coprecipitation method. In the present investigation, ZnO nanoparticles and Mn-doped ZnO nanoparticles are synthesized and the effect of Mn dopant on its structural, morphological, optical and antibacterial activity properties has been studied and discussed in detail.

2. Materials and methods

2.1 *Synthesis process*

The ZnO:Mn nanoparticles were synthesized using simple coprecipitate method. Zinc acetate dihydrate ($Zn(CH_3COO)_2{\cdot}2H_2O$) (0.2 M) and manganese acetate tetrahydrate ($Mn(CH_3COO)_2{\cdot}4H_2O$) (10%) were used as doping precursors. The pH value was maintained at 8.5 by adding required amount of NaOH solution to the starting solution. The prepared solution was magnetically stirred for about 2 h at 85°C. After the completion of the stirring process, the resultant solution was cooled to room temperature and kept undisturbed for 1 h to get the required precipitate. Then, it was filtered and washed separately with a mixture of ethanol and water kept in the ratio of 1 : 3. Finally, the product was calcinated at 500°C for 4 h to get it in the powder form.

The XRD spectra were recorded using Bruker D8 advanced XRD with CuKα1 (1.54060 Å) as a source. The SEM micrographs of the experimental samples have been obtained using scanning electron microscope (INPECT-F Model). The absorbance of ZnO was measured at room temperature using spectrophotometer (Shimadzu UV-Vis 1800). Besides, the photoluminescence spectra of ZnO nanoparticles were also recorded by Spectrofluorometer (Perkin Elmer LS55).

2.2 *Evaluation of antibacterial performance*

The antibacterial property of undoped ZnO and Mn-doped ZnO nanoparticle were analysed by their zone of inhibitions for *Escherichia coli* (*E. coli*), *Klebsiella pneumonia* (*K. pneumonia*), *Pseudomonas aeruginosa* (*P. aeruginosa*), *Staphylococcus aureus* (*S. aureus*), *Salmonella typhimurium* (*S. typhimurium*) and *Streptococcus agalactiae* (*S. agalactiae*). An overnight culture of each organism was adjusted to an OD of 0.1 and swabbed onto Mueller Hilton agar plates. These plates were incubated at 37°C for 24 h and 48 h. The zone of inhibitions was measured in diameter.

3. Results and discussion

3.1 *Structural properties*

(a) XRD Analysis

Figure 1 shows a typical XRD pattern of the synthesized uncapped ZnO and Mn-doped ZnO nanopowder. The peaks correspond to the Miller indices (1 0 0),

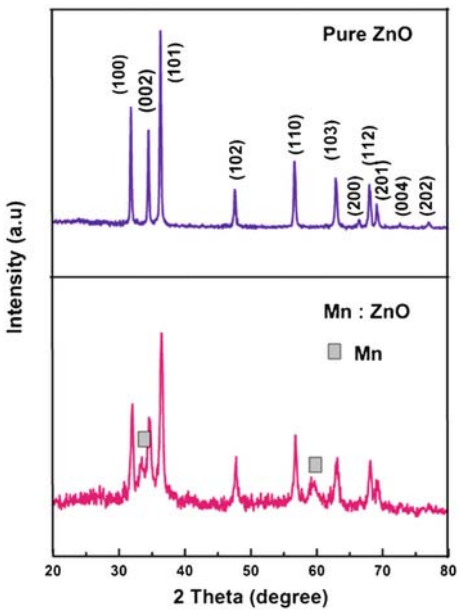

Figure 1. XRD pattern of synthesized pure ZnO and Mn-doped ZnO nanoparticles.

(0 0 2), (1 0 1), (1 0 2), (1 1 0), (1 0 3), (2 0 0), (1 1 2), (2 0 1), (0 0 4) and (2 0 2) and Bragg angles 31.78°, 34.44°, 36.26°, 47.55°, 56.60°, 62.87°, 66.34°, 67.97°, 69.09°, 72.54° and 76.92°. These peaks are sharp and highly intense. The strongest diffraction peak shows that the preferential orientation is along the (1 0 1) plane. All the indexed peaks match well with the JCPDS No. 36-1451. This confirms the wurtzite hexagonal structure of ZnO with lattice parameters $a = 3.2451$ Å and $c = 5.1901$ Å. In the Mn-doped ZnO nanoparticles, the intensity decreases. Further, two peaks are newly presented at $2\theta = 33.4$ and 59. Moreover, a slight variation was observed in the peak broadening and intensity. The peak broadening clearly indicates the formation of small-sized particles. Similar behaviour is exhibited by ZnO nanoparticles which has been reported earlier [21]. The grain sizes are compared to the pure ZnO and Mn-doped ZnO nanoparticles. The grain sizes (D) of the crystallites were calculated using the Debye–Scherrer's formula [22].

$$D = 0.94(\lambda/\beta\cos\theta), \tag{1}$$

where λ is the wavelength of CuKα used, β is the full-width at half-maximum of the peak position in radian and θ is the Bragg diffraction angle at the peak position in degrees. The lattice constants a and c are calculated using the formula [23,24]

$$\frac{1}{d^2} = \frac{4}{3}\left[\frac{h^2 + hk + l^2}{a^2}\right] + \frac{l^2}{c^2}, \tag{2}$$

where d is the interplanar spacing (d-spacing) value and (h, k, l) are the Miller indices. The calculated lattice constants a and c are very close to that of the standard values (JCPDS: 36-1451) for both ZnO and Mn-doped ZnO nanoparticle. These results show that the lattice constants are not affected much by the substitutional incorporation of Mn into the O sites. The volume of the unit cell (v) is estimated using the relation [25]

$$v = \left[\frac{\sqrt{(}3)}{2}\right] a^2 c. \tag{3}$$

The volume of a crystallite (V) is calculated using the relation

$$V = D^3. \tag{4}$$

From the volume of the unit cell and the volume of the crystallite, we can estimate the number of unit cells per crystallite (N_u) using the equation,

$$N_u = \frac{V}{v}. \tag{5}$$

The estimated values (table 1) clearly showed that the decrease in the number of unit cells per crystallite (N_u) as seen in table 1 is an expected result, as the incorporation of Mn disturbs the possible grouping of a large number of unit cells into a crystallite.

Atomic packing fraction (APF) was calculated using formula

$$\text{APF} = \frac{2\pi a}{3\sqrt{(}3)c}, \tag{6}$$

where a and c are the lattice parameters. The values of APF are listed in table 1. The APF of bulk hexagonal ZnO materials is about 74% but in our case the APF of pure ZnO and Mn-doped ZnO nanoparticles is nearly 75% in hexagonal structure. It means that APF in nanocrystals are slightly larger than that of bulk materials.

The values of D are presented in table 1 along with the lattice constants a, c and c/a, volume of the unit cell, volume of the crystallite and number of unit cells in a crystallite. Table 1 clearly shows that the crystallite size (D) decreases with the higher Mn doping level (10%) for Mn-doped ZnO samples as shown by various researchers [31–34]. This result must be a consequence of the increase in the Mn incorporation in the ZnO lattice with the increase in the doping level. This interpretation can be explained on the basis of the fact that a crystallite is an aggregate of a number of unit cells arranged in a periodic manner. This partial reduction in crystallite size with the higher doping level as seen in table 1 is an expected result, as the incorporation of Mn disturbs the possible grouping of a large number of unit cells into a crystallite.

3.2 *Morphological analysis*

The surface morphologies of the pure ZnO and Mn-doped ZnO nanoparticles were investigated by scanning electron microscope (SEM). Figures 2a and 2b show ZnO nanoparticles (3 μm and 500 nm). SEM studies show that the materials are networks of rod-like crystals. The images show that all the samples have micrometric structure and well-defined grains with hexagonal cross-section, and the structures obtained are similar to the structure reported by Kim *et al* [26]. SEM images of figure 2a show a rod-shaped ZnO in different sizes and figure 2b exhibits a small rod shaped smooth surface of a solid, unless this is the effect of agglomeration. Figures 2c and 2d indicate (3 μm and 1 μm) Mn-doped ZnO nanoparticles which are rod-shaped. The addition of Mn affected the surface morphology and prevented agglomeration. SEM

Table 1. Structural parameters of ZnO:Mn nanoparticles.

Sample	Lattice constants[a] (Å)			Crystallite size (D) (nm)	Volume of the unit cell (v) (Å^3)	Volume of the crystallite (V)$\times 10^3$ (nm^3)	(N_u)$\times 10^6$	APF
	a	b	c					
Undoped ZnO	3.2451	5.1901	1.5994	39	47.33	59.32	1.2533	0.7553
Mn-doped ZnO	3.2594	5.2073	1.5976	20	47.91	8.000	0.1670	0.7561

[a]Standard values: $a = 3.248$ Å and $c = 5.206$ Å (JCPDS card no. 36-1451). Error values (ZnO): $a = 0.0029$ Å and $c = 0.0159$ Å. ZnO:Mn: $a = -0.0114$ Å, $c = -0.0013$ Å.

studies show that the materials are network of hexagonal crystals. The structures obtained are similar to structures reported by earlier researchers [27].

3.3 *UV–Vis spectroscopy*

The UV–Vis spectra of pure and Mn-doped ZnO are shown in figure 3. The pure ZnO exhibits its absorption peak at 362 nm. The Mn-doped ZnO exhibits slightly blue shifted peak at 360 nm. The blue shift in the absorption spectrum edge is a clear indication of the incorporation of Mn inside the ZnO lattice. It may be the strain due to Mn doping that causes the change in the band structure of doped ZnO resulting in blue shift. We have also observed an increase in absorption intensity in ultraviolet region of the spectrum with the Mn doping sample region, all the samples exhibit decrease in intensity of absorption spectra compared to pure ZnO.

As in the semiconducting materials, the optical band gap energy (E_g) is defined as the energy at which the absorption coefficient has a value $>10^4$ cm^{-1}. In order to find the value of E_g for our samples, we use the Tauc relation [28,29].

$$\alpha h\nu = A(h\nu - E_g)^m, \tag{7}$$

where α is the absorption coefficient given by $\alpha = 2.303\log(T/d)$ (d is the thickness of the sample and T is the transmission) and $h\nu$ is the photon energy. Figure 4 shows the plots of $(\alpha h\nu)^2$ vs. $h\nu$ for pure ZnO and Mn-doped samples. Linearity of the plots indicates that the material is of direct band-gap nature. The values of E_g have been estimated by taking the intercept of the extrapolation to zero absorption with photon energy axis i.e., $(\alpha h\nu)^2 \to 0$. The E_g is found to be 3.20 eV for pure ZnO sample and increases with Mn doping and a value of 3.25 eV is estimated for Mn concentration, only 10% as shown in figure 4.

This change in the value of E_g depends on several factors such as grain size, carrier concentration, lattice strain, size effect etc. Because the particle sizes of the samples in the present study are much bigger than the sizes for which quantum confinement effect occurs, the observed shifting cannot be assigned to the size effect. This blue-shift behaviour or increase in the band gap may be attributed to the fact that any change in the band gap of Mn-doped ZnO depends on orbitals hybridized between Mn atom and the host band. Because the band gap of MnO (bulk band gap = 4.2 eV), is greater than that of ZnO (bulk band gap = 3.37 eV, error value for undoped ZnO is 0.17 eV and for Mn-doped ZnO is

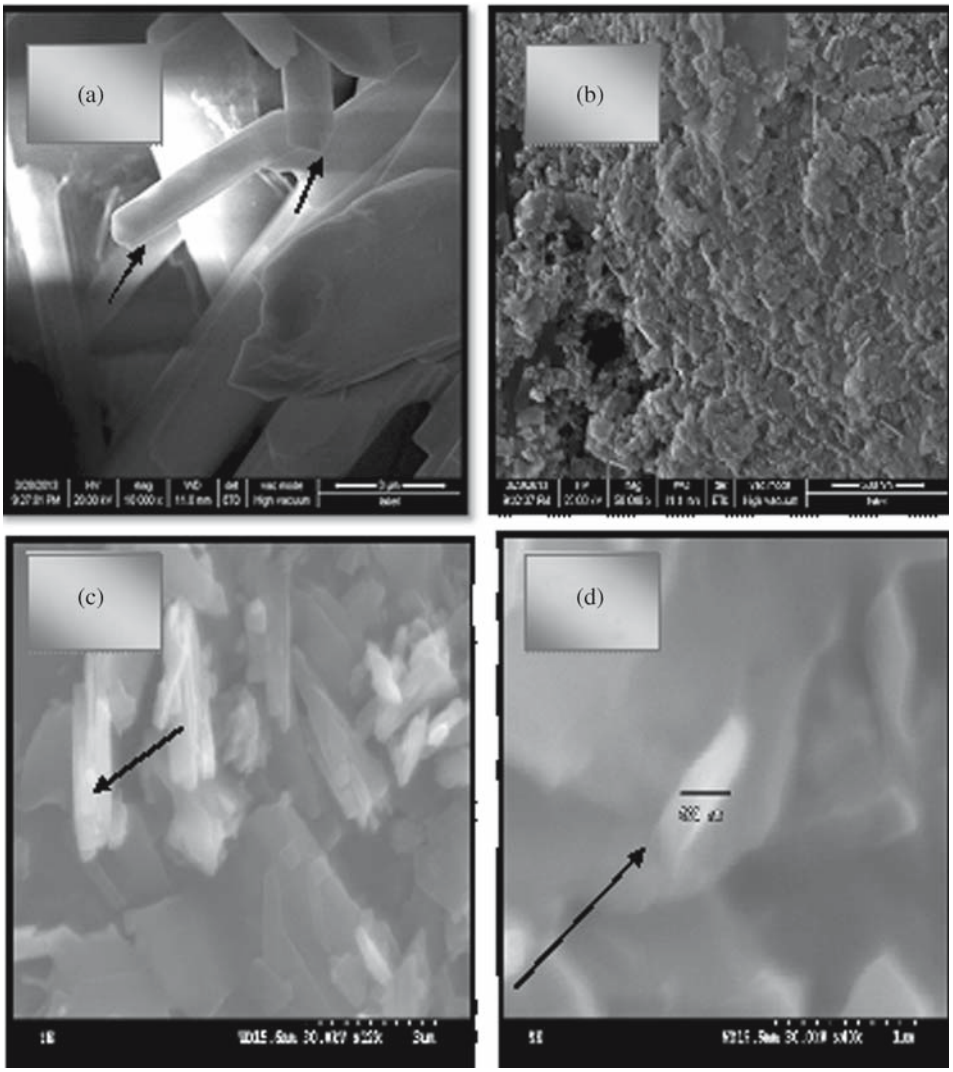

Figure 2. (**a**) and (**b**) show SEM images for rod-shaped pure ZnO and (**c**) and (**d**) show Mn-doped ZnO nanoparticle.

0.12 eV), it is reasonable to expect that the band gap increases with the addition of Mn [30].

3.4 *FTIR spectra*

Fourier transform infrared spectroscopy of ZnO and ZnO:Mn nanoparticles has been used to determine the presence of vibrational bands in the prepared samples. FTIR spectra of ZnO and ZnO:Mn nanoparticles are shown in figure 5. Normally, the FTIR spectra give information about the presence of functional groups, molecular geometry and inter- or intramolecular interactions in the prepared samples. It is observed that the presence of band frequencies in the range between 0 and 1000 cm^{-1} may be due to the bond between inorganic elements in the prepared sample. The observation of strong peak at 450 cm^{-1} may be assigned to stretching vibration of ZnO which confirmed the wurtzite structure of the prepared samples [31,32]. The appearance of peak at 677 cm^{-1} in figure 5b may be due to the vibration mode of MnO which is not observed in figure 5a for pure ZnO. It is also observed that the appearance of band at 1016, 1200 and 1600 can be attributed to C–O (stretching), C=O (asymmetric stretching), C=C (asymmetric stretching due to Lewis acidity), C=O (symmetric stretching due to Bronsted acidity) group that are present in the citrates species on the surface of the nanoparticles. The peaks observed at 2360 and 2921 cm^{-1} may be due to the presence of CO_2 molecule in acetate, air and C–H stretching mode, respectively. It is found that the appearance of broad absorption peak at 3451 cm^{-1} is attributed to the O–H group of H_2O, indicating the existence of water absorbed on the surface of nanocrystalline powders. The vibration frequency

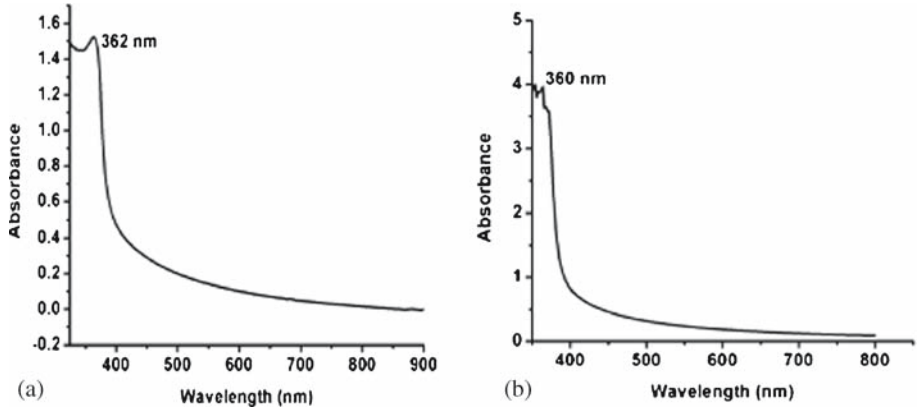

Figure 3. Absorption spectra of pure and Mn-doped ZnO nanoparticles.

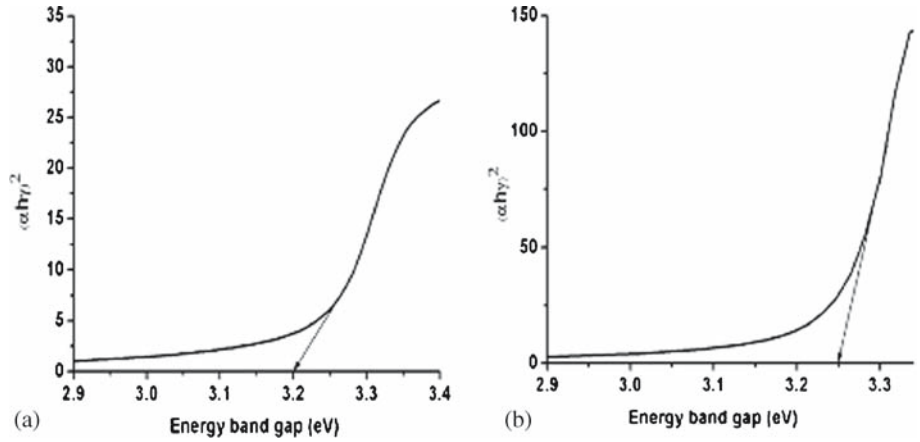

Figure 4. The plot of $(\alpha h\nu)^2$ vs. $h\nu$ for (**a**) pure ZnO and (**b**) Mn-doped ZnO nanoparticles.

values of the corresponding modes for both ZnO and ZnO:Mn nanoparticles are given in table 2.

3.5 *Photoluminescence study*

Photoluminescence analysis is a powerful tool to understand the nature of defects of the synthesized nanopowders. The photoluminescence spectra of undoped and Mn-doped ZnO nanopowders obtained in the range of 350–525 nm at room temperature under the excitation wavelength of 325 nm are shown in figure 6. PL spectra of ZnO and Mn-doped ZnO nanoparticles are shown in figure 6. The spectra of the nanoparticles include four main emission bands: a strong UV emission band at 394 and 384 nm, a weak blue band at 458 nm, a weak blue–green band at 490 nm and a very weak green band at 530 nm. The strong UV emission corresponds to the exciton recombination related to the near-band edge emission of ZnO. The weak blue and weak blue–green emissions are possibly due to the surface defects in the nanoparticles as in the case of ZnO nanomaterials reported by other researchers [33]. The weak green band emission corresponds to the singly ionized oxygen vacancy in ZnO. This emission results from the recombination of a photogenerated hole with the singly ionized charge state of the specific defect. Compared to Mn-doped ZnO nanoparticles, the low intensity of the green emission of ZnO nanoparticles may be due to the low density of oxygen vacancies during the preparation, whereas, the strong UV emission intensity should be attributed to the high purity and perfect crystallinity of the synthesized nanoparticles [34].

3.6 *Antibacterial studies*

The antibacterial activity of ZnO:Mn nanoparticles having two different time period was estimated using the zone of inhibition method. Bacterial strains of *E. coli*, *K. pneumonia*, *P. aeruginosa*, *S. aureus*, *S. typhimurium* and *S. agalactiae* were used for the antibacterial test. From figure 7, it is observed that doped ZnO samples prevented the growth of bacteria remarkably and formed well-defined zones around the

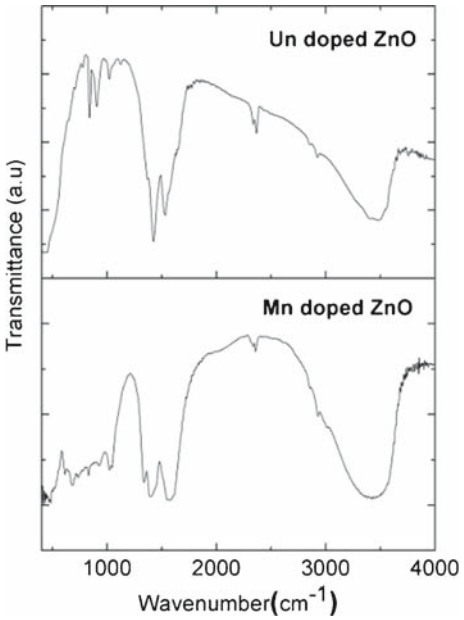

Figure 5. FTIR spectra of (**a**) pure ZnO and (**b**) Mn-doped ZnO at room temperature.

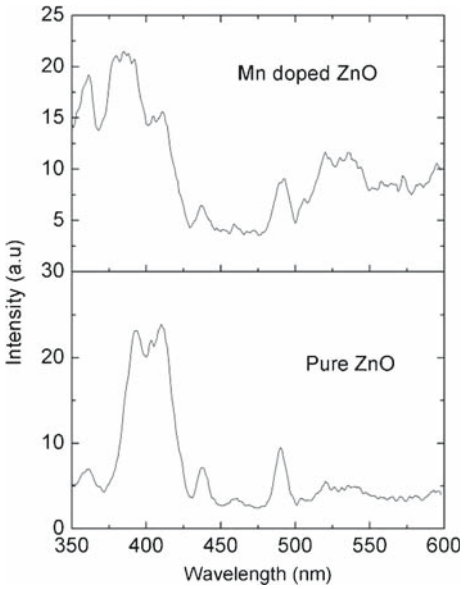

Figure 6. Photoluminescence spectra of pure ZnO and Mn-doped ZnO under an excitation wavelength of 325 nm at room temperature.

Table 2. FTIR vibration frequencies for different modes of pure ZnO and Mn-doped ZnO.

Undoped Zno	Mn-doped ZnO	Vibration modes
450	450	Zn−O
–	677	Mn−O
848	–	Zn−O
900	–	Zn−O
1036	1036	C−O stretching vibration
1425	1393	C=O symmetric stretching
1534	1566	C=O asymmetric stretching
2360	2360	CO_2 molecule
2921	2921	C−H bond stretching
3451	3451	O−H bond

samples. Moreover, the zone of inhibition for the individual micro-organisms increases with the increase in the period of time. The antibacterial activity of the ZnO nanoparticles may be related to several mechanisms including the generation of reactive oxygen species (ROS) on the surface of the particles [35], release of Zn^{2+} ions from the ZnO samples and the penetration of these nanoparticles which contributes to the mechanical destruction of cell membrane [36]. The hydroxyl radicals and superoxide anions are negatively charged and hence they cannot penetrate into the cell membrane, but they can cause fatal damage to proteins, DNA and lipids, whereas, H_2O_2 can penetrate directly into the cell wall and kill the bacteria [37]. In the present work, the antibacterial activity is against *E. coli*, *K. pneumonia*, *P. aeruginosa*, *S. aureus*, *S. typhimurium* and *S. agalactiae*. The increase in the zone of inhibition is caused by the substitution of Mn ions into the Zn ion sites; The ROS can rupture the cell membrane and kill the bacteria. Mn-doped ZnO nanopowder in the starting solution can enhance the possibility of interstitial incorporation of Mn and Zn ions into the ZnO lattice.

The increased intensity in the blue emission at 425 nm (2.92 eV) observed in the PL spectra at Mn-doped ZnO is a clear evidence for these interstitial incorporations (figure 7). These interstitial incorporations cause the generation of free carriers in the lattice. These free carriers in turn result in an improvement in the antibacterial efficiency. The reduction in the crystallite size as estimated from the X-ray diffraction data (table 1) and the reduction in the grain size of Mn-doped ZnO confirmed from SEM images (figure 2) provide more contact area for micro-organism. This could be another reason for the improved antibacterial activity compared to that of the undoped ZnO. With increase in the time duration after 48 h, the diameters of the zone of inhibition increased for both ZnO and Mn-doped ZnO (figure 7). The maximum antibacterial activity was shown on the *E. coli* and *K. pneumonia* followed by *P. aeroginosa*, *S. auereus*, *S. typhimurium* and *S. agalactiae*. In the present investigation, ZnO and

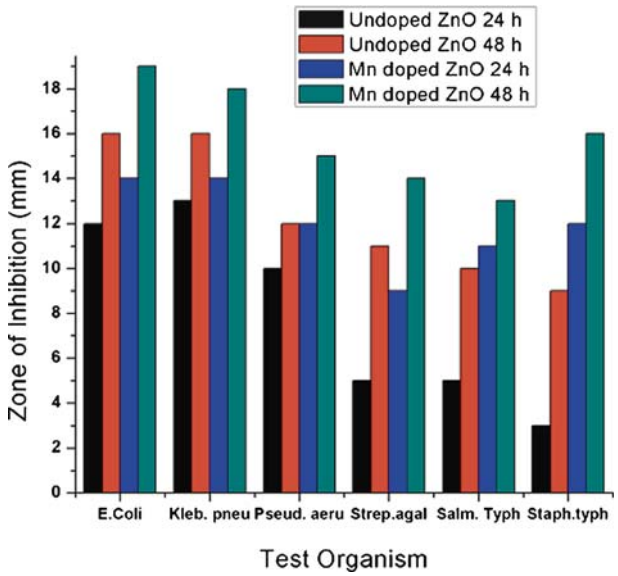

Figure 7. Inhibition zones caused by ZnO:Mn nanoparticles against six different pathogenic bacterias.

Mn-doped ZnO nanoparticles having high antibacterial activity against *E. coli* was investigated.

4. Conclusion

ZnO and Mn-doped ZnO nanoparticles with hexagonal crystal structure were synthesized by coprecipitate method and were characterized by XRD, SEM, FTIR, UV–Vis and photoluminescence spectroscopy. Results of XRD analysis revealed average crystalline size of 39 and 20 nm for ZnO and Mn-doped ZnO nanoparticles, respectively. The absorption studies confirmed the existence of manganese at zinc sites in Mn-doped ZnO nanoparticles. UV–Vis studies revealed that the optical band-gap energy is 3.20 and 3.25 eV for ZnO and Mn-doped ZnO nanoparticles respectively. Room-temperature photoluminescence spectra of the samples showed four main emission bands including a strong UV emission band, a weak blue band, a weak blue–green band and a weak green band indicating their high structural and optical qualities. Such luminescent, magnetic nanoparticles with biocompatible dopant can have diverse applications in biology, pharmaceuticals and medicine. The Mn-doped ZnO nanoparticles show better antibacterial activity against the *E. coli* bacteria than against others when doping level is higher (10 at%) and duration of time is longer. This better antibacterial efficiency at higher doping levels is due to the interstitial incorporation of Mn and Zn, the resultant increase in the carrier concentration and the decrease in the crystallite size and grain size values as evidenced by the PL, UV–Vis, XRD and SEM results.

References

[1] U Desselberger, *J. Infect.* **40**, 3 (2000)
[2] J S Kim, E Kuk, K N Yu, J H Kim, S J Park, H J Lee, S H Kim, Y K Park, Y H Park, C Y Hwang, Y K Kim and Y S Lee, *Nanomedicine* **3**, 95 (2005)
[3] K R Raghupathi, R T Koodali and A C Manna, *Langmuir* **27**, 4020 (2011)
[4] J Liu, Z Guo and F L Meng, *Cryst. Growth Des.* **9**, 1716 (2009)
[5] K Ravichandran, R Mohan, N Jabena Begum, K Swaminathan and C Ravidhas, *J. Phys. Chem. Solids* **74**, 1794 (2013)
[6] B Sundaresan, A Vasumathi, K Ravichandran, P Ravikumar and B Sakthivel, *Surf. Eng.* **28**, 323 (2012)
[7] X S Tang, E Shi, G Choo, L Li, J Ding and J M Xue, *Chem. Mater. Am. Chem. Soc.* **22**, 3383 (2010)
[8] H Wang and C Xie, *J. Phys. Chem. Solids* **69**, 2440 (2008)
[9] M Ladanov, P Algarin-Amaris, P Villalba, Y Emirov, G Matthews, S Thomas, K Ram, A Kumar and J Wang, *J. Phys. Chem. Solids* **74**, 1578 (2013)
[10] S H Chen, J X Ji, Q Lian, Y L Wen, H B Shen and N Q Jia, *Nano Biomed. Eng.* **2**, 15 (2010)
[11] K W Chae, Q Zhang, J S Kim, Y H Jeong and G Cao, *J. Nanotechnol.* **1**, 128 (2010)
[12] X Y Ma and W D Zhang, *Polym. Degrad. Stab.* **94**, 1103 (2009)
[13] S Chakraborty, A K Kole and P Kumbhakar, *Mater. Lett.* **67**, 362 (2012)
[14] M S Niasari, F Davar and A Khansari, *J. Alloys Compd.* **509**, 61 (2011)
[15] J Yang, L Fei, H Liu, Y Liu, M Gao, Y Zhang and L Yang, *J. Alloys Compd.* **509**, 3672 (2011)
[16] Y Yang, H Chen, B Zhao and X Bao, *J. Crystal Growth* **263**, 447 (2004)
[17] J Q Hu, Q Li, N B Wong, C S Lee and S T Lee, *Chem. Mater.* **14**, 1216 (2002)
[18] J Y Lao, J Y Huang, D Z Wang and Z F Ren, *Nano Lett.* **3**, 235 (2003)
[19] R Chauhan, A Kumar and R P Chaudharya, *J. Chem. Pharm. Res.* **2**, 178 (2010)
[20] R Savu, R Parra, E Joanni, B Jancar, S A Elizario, R de Camargo, P R Bueno, J A Varela, E Longo and M A Zaghate, *J. Crystal Growth* **311**, 4102 (2009)
[21] O D Jayakumar, I K Gopalakrishnan, R M Kadam, A Vinu, A Asthana and A K Tyagi, *J. Crystal Growth* **300**, 358 (2007)
[22] V Senthamilselvi, K Saravanakumar, N Jabena Begum, R Anandhi, A T Ravichandran, B Sakthivel and K Ravichandran, *J. Mater. Sci.: Mater. Electron.* **23**, 302 (2012)
[23] R Anandhi, R Mohan, K Swaminathan and K Ravichandran, *Superlatt. Microstruct.* **51**, 680 (2012)
[24] B D Cullity, *Elements of X-ray diffraction* (Addison-Wesley Publishing Company, 1978)

[25] A Goswami, *Thin film fund* (New Age International (P) Ltd Publications, New Delhi, 2005)
[26] S Jung Kim and D W Park, *Appl. Surf. Sci.* **255**, 5363 (2009)
[27] D Jung, *Solid State Sci.* **12**, 466 (2010)
[28] G Elilarassi and J Chandrasekaran, *Mater. Sci. Mater. Electron.* **21**, 1168 (2010)
[29] S Suwanboon, P Amornpitoksuk, A Haidoux and J C Tedenac, *J. Alloys Compd.* **462**, 335 (2008)
[30] R Viswanatha, S Sapra, S Gupta, B Satpati, P V Satyam, B N Dev and D D Sarma, *J. Phys. Chem. B* **108**, 6303 (2004)
[31] P D Cozzoli, M L Curri, A Agostiano, G Leo and M Lomascolo, *J. Phys. Chem. B* **107**, 4756 (2003)
[32] Y Guo, X Cao, X Lan, C Zhao, X Xue and Y Song, *J. Phys. Chem. C* **112**, 8832 (2008)
[33] W I Park, G C Yi and H M Jang, *Appl. Phys. Lett.* **79**, 2022 (2001)
[34] S Maensiri, C Masingboon, V Promarak and S Seraphin, *Optik. Mater.* **29**, 1700 (2007)
[35] M Vasanthi, K Ravichandran, N Jabena Begum, G Muruganantham, S Snega, A Panneerselvam and P Kavitha, *Superlatt. Microstruct.* **55**, 180 (2013)
[36] L Zang, Y Jiang, Y Ding, M Povey and D York, *J. Nanopart. Res.* **9**, 479 (2007)
[37] N Padmavathy and R Vijayaraghavan, *Sci. Technol. Adv. Mater.* **9**, 035004 (2008)